CHEMICAL ENGINEERING TRANSACTIONS
VOL. 109, 2024
A publication of AIDIC
The Italian Association of Chemical Engineering
Online at www.cetjournal.it
Guest Editors: Leonardo Tognotti, Rubens Maciel Filho, Viatcheslav Kafarov

ISBN 979-12-81206-09-0; **ISSN** 2283-9216
DOI: 10.3303/CET24109048

Effect of pH and Applied Bias on H_2 and HVA Products Through Photoelectrocatalytic Glycerol Oxidation

Claudio M. Pecoraro*, Francesco Di Franco, Vittorio Loddo, Marianna Bellardita, Monica Santamaria

Dipartimento di Ingegneria, Università degli Studi di Palermo, Viale delle Scienze Edificio 6, 90128 Palermo, Italy
claudiomaria.pecoraro@unipa.it

This study explores how pH and applied bias influence the generation of H_2 and high-value-added products resulting from glycerol photooxidation, specifically targeting 1,3-dihydroxyacetone (DHA) and glyceraldehyde (GA), within a photoelectrochemical cell. TiO_2 NTs with a length of 760 nm were utilized as the photoanode, while Ni foam served as the cathode. The experiments were carried out under acidic, neutral, and alkaline pH conditions, with applied biases ranging from 0.1 to 1 V vs. Ag/AgCl reference electrode.
The findings demonstrated that the highest faradaic efficiency towards high-value-added products, namely DHA and GA, was achieved at pH 7 with an applied bias of 0.5 V vs. Ag/AgCl, and this efficiency remained stable at higher bias values. Notably, at pH levels of 2 and 7, both glycerol mineralization into CO_2 and H_2, and glycerol photooxidation into DHA and GA were more pronounced. Conversely, at higher pH, the faradaic efficiency towards DHA, GA, and CO_2 decreased, while the photocurrent increased. This observed trend suggests a heightened water splitting effect at higher pH, leading to a reduction in faradaic efficiency towards H_2 due to subsequent reactions with O_2 in the gas phase.
Keywords: Glycerol partial oxidation, H_2 production, Photoelectrocatalysis, TiO_2 nanotubes, Pt-free cathode

1. Introduction

In recent years, the increasing energy demands, and subsequent CO_2 emissions have led to significant efforts towards renewable and low-carbon energy sources. In this context, an emerging opportunity involves harnessing biomasses to simultaneously produce hydrogen and valuable products (Pecoraro et al., 2024).
Among the available biomasses, glycerol, a biodiesel production byproduct, has obtained increasing attention for its ability to yield hydrogen and valuable compounds like 1-3 dihydroxyacetone (DHA) and glyceraldehyde (GA) (Pecoraro et al., 2023), fundamental in industries such as cosmetics, pharmaceuticals, fine chemicals, and food production (Kong et al., 2016). Consequently, the production of DHA and GA from glycerol represents an economically attractive option (Luo et al., 2022).
Traditional methods of producing DHA and GA from glycerol involve thermo-catalysis under harsh conditions, needing costly noble-metal catalysts (e.g., Pt, Au, Pd), and external oxidants like O_2 or H_2O_2 (Verma et al., 2022). To minimize energy consumption, light-based approaches like photoelectrocatalysis (PEC) have emerged, offering a sustainable pathway to oxidize organic compounds, generate valuable chemicals, and promote cathodic H_2 production. This technique couples photocatalysis and electrocatalysis, using semiconductor photoelectrodes irradiated with light having energy higher than their band gap, while the exposition to an electric potential effectively separates the photo-produced species (Yao et al., 2018). In PEC systems, photo-produced electrons (e^-) and holes (h^+) migrate to the cathode and the photocatalyst surfaces respectively, triggering reduction and oxidation reactions at these spots (Pitchaimuthu et al., 2022). Although PEC research primarily focuses on water splitting and breaking down pollutants, it is a sustainable way to oxidize organic compounds, producing valuable chemicals and encouraging cathodic H_2 production (Dey et al., 2021). Notably, in PEC oxidation of glycerol to DHA and GA, the achievement of high FE remains an actual challenge. In this work, the effect of pH and applied bias on hydrogen production by glycerol photoreforming and water splitting was studied to enhance both the hydrogen evolution rate and the FE towards DHA and GA. A special

Paper Received: 16 December 2023; Revised: 22 February 2024; Accepted: 27 March 2024
Please cite this article as: Pecoraro C.M., Di Franco F., Loddo V., Bellardita M., Santamaria M., 2024, Effect of Ph and Applied Bias on H2 and Hva Products Through Photoelectrocatalytic Glycerol Oxidation, Chemical Engineering Transactions, 109, 283-288 DOI:10.3303/CET24109048

attention was paid to the development of a photoelectrochemical cell employing both PGM-free cathode and photoanode to point towards low-cost alternative materials compared to the noble metal-based catalysts and to overcome possible poisoning effects due to the presence of organic species. As supplied commercial Ni foam was used as cathode. The photoanode was prepared by anodizing Ti foils in a fluoride containing electrolyte to induce the growth of large arrays of well aligned TiO_2 nanotubes in the attempt to widen the active surface of the electrode. Photoelectrochemical tests were carried out to assess the formation of a n-type semiconducting material, while electrochemical impedance measurements allowed to study the behavior of the photoanode/electrolyte interface under irradiation. The concentration of H_2 in the gas phase was monitored by gas chromatography (GC), while high performance liquid chromatography (HPLC) was used to determine the concentration of DHA and GA in the liquid phase.

2. Experimental

TiO_2 NTs were grown on Ti foil (purity > 99.7 % and 0.127 mm thickness, Sigma Aldrich). Ti foil was cut and etched in a solution containing hydrofluoric acid (Sigma Aldrich, 39.5 %), nitric acid (Sigma Aldrich, 69 %), and deionized water in 1:1:3 volume ratios for 15 seconds. Then, it was cleaned in acetone and ethanol through ultrasonic treatment for 5 minutes each and rinsed with deionized water before being dried in air. The TiO_2 nanotubes were formed in an ethylene glycol (Sigma Aldrich, 99.8 % anhydrous) solution containing 0.25 %wt NH_4F (Sigma Aldrich, ≥ 98 %) and 0.75 %wt deionized water. The anodization of 25 cm^2 of immersed surface was performed using a two-electrode configuration with aluminum foil as the cathode and maintaining a constant potential of 45 V for 10 minutes. Post-anodizing, annealing at 450°C for 3 hours under air exposure was carried out to induce crystallization in the TiO_2 nanotubes. The cathode employed in the process was 6 cm^2 of commercial Ni foam (Goodfellow).
SEM images were captured using an FEI Quanta 200 ESEM microscope operating at 30 kV. XRD patterns of the photoanodes were obtained at room temperature using a PANalytical Empyrean diffractometer equipped with a PIXcel1D detector. The diffractometer operated at 40 kV and 40 mA using CuKα radiation, with a 2θ scan rate set at 3°/min. Raman spectra were carried out using a Raman Microscope coupled with a Leica DMLM microscope.
Photocurrent transients were carried out by using TiO_2 NTs as the working electrode within a three-electrode setup. A Pt wire was used as the counter electrode, while an Ag/AgCl/saturated KCl setup was the reference electrode. The electrolyte consisted of a 0.5 M Na_2SO_4 aqueous solution. Current transients were recorded using monochromatic irradiation at different constant potentials. The photocurrent (I_{ph}) was quantified by manually stopping the irradiation while maintaining the applied potentials steady, ranging from 0.5 V to -0.5 V vs Ag/AgCl.

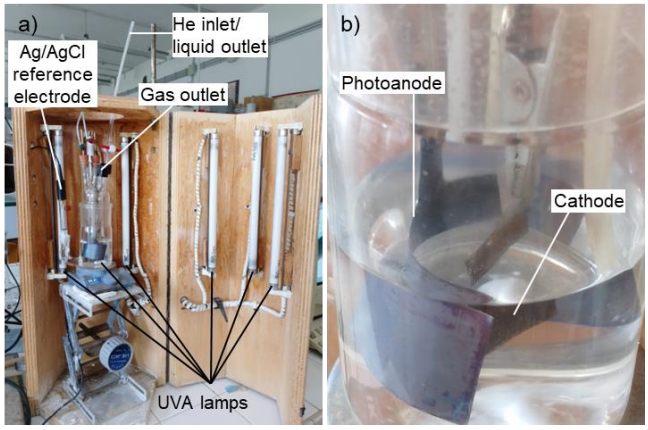

Figure 1: a) overview of the experimental setup and b) magnification of photoanode and cathode

EIS measurements were carried out in 0.5 M Na_2SO_4 aqueous solution employing a Parstat 2263 potentiostat featuring an Impedance Analyzer connected to the cell setup. The impedance spectra were obtained in a frequency range of 10 kHz to 0.1 Hz at 25 °C, using an AC amplitude of 10 mV. Before each measurement, the cell underwent a stabilization period of at least 15 minutes under irradiation. Subsequently, data analysis and fitting of the equivalent circuit were performed utilizing Power Suite and ZSimpleWin software.
Photoelectrocatalytic experiments were carried out in a 450 ml undivided glass cell by using three electrodes as shown in Figure 1.

The setup used Ni foam as the counter electrode and an Ag/AgCl electrode as the reference. The solution underwent external illumination from six UVA fluorescent lamps emitting light at a maximum wavelength of 365 nm (8 W). Before each test, Helium was bubbled through a 150 ml aqueous solution for approximately 30 minutes. The control over the cell potential was maintained by using a CH Instrument 630B Series potentiostat. A 0.5 M Na_2SO_4 solution was used as the electrolyte (pH ~ 7), the glycerol starting concentration was 0.1 M, and an applied potential up to 1 V vs Ag/AgCl was employed. To study the effect of the pH, H_2SO_4 was added dropwise, or a KOH solution was used as the electrolyte. The quantification of glycerol and the concentration of reaction intermediates was performed by using a Thermo Scientific Dionex UltiMate 3000 HPLC, equipped with a Diode Array detector and a REZEK ROA Organic acid H^+ column. The analysis of gaseous species accumulated in the reactor headspace was carried out by using an HP 6890 Series GC system equipped with a Supelco GC 60/80 CarboxenTM-1000 packed column and a thermal conductivity detector. The FE towards the products was calculated using Eq. (1).

$$\boldsymbol{Faradic\ efficiency_i}\ [\%] = \frac{\boldsymbol{Amount\ of\ product\ i\ formed}\ [\boldsymbol{mol}]}{\frac{\boldsymbol{Q}\ [\boldsymbol{Coulomb}]}{\boldsymbol{z\ F}\left[\boldsymbol{Coulomb}/_{\boldsymbol{mol}}\right]}}\ \boldsymbol{x\ 100} \tag{1}$$

where:
- i is the formed product
- Q is the circulated charge
- z are the electrons exchanged, equal to 2 for H_2, DHA, and GA and 14/3 for CO_2 according to the anodic and cathodic semi-reactions in Eqs. (2-4)
- F is the Faraday constant of 96485 [Coulomb/mol]

$$\boldsymbol{Photoanode}: \boldsymbol{C_3H_8O_3 + 2h^+ \rightarrow C_3H_6O_3 + 2H^+} \tag{2}$$

$$\boldsymbol{Photoanode}: \boldsymbol{C_3H_8O_3 + 3H_2O + 14h^+ \rightarrow 3CO_2 + 14H^+} \tag{3}$$

$$\boldsymbol{Cathode}: \boldsymbol{2H^+ + 2e^- \rightarrow H_2} \tag{4}$$

where $C_3H_6O_3$ is DHA or GA.

3. Results and discussion

Figure 2a shows the SEM image of TiO_2 NTs after the anodization and annealing steps. The micrograph distinctly exhibits the successful growth of a large array of TiO_2 NTs, showing an average length of 760 nm approximately, in line with previous results (Santamaria et al., 2017). The XRD pattern presented in Figure 2b shows distinct peaks corresponding to bare titanium (Reyes-Coronado et al., 2008), whereas the Raman spectra depicted in Figure 2c exhibits distinctive peaks corresponding to anatase at 144 cm^{-1}, 196 cm^{-1}, 397 cm^{-1}, 513 cm^{-1}, and 639 cm^{-1} (Balachandran et al. 1982). According to previous findings, the annealing process involves two concurrent phenomena. Firstly, the amorphous TiO_2 within the nanotubes transforms into anatase, while the underlying layer at the interface between titanium and the nanotubes to rutile. This formation of rutile promotes a strong adhesion between the nanotubes and the metallic substrates. When the system is subjected to a thermal treatment at 450°C in an air environment for 3 hours, it results in a 140 nm thick rutile layer. Furthermore, the nanotube wall primarily consists of anatase crystals with a cylindrical morphology, extending several hundred nanometers along the nanotube axis (Albu et al., 2010).

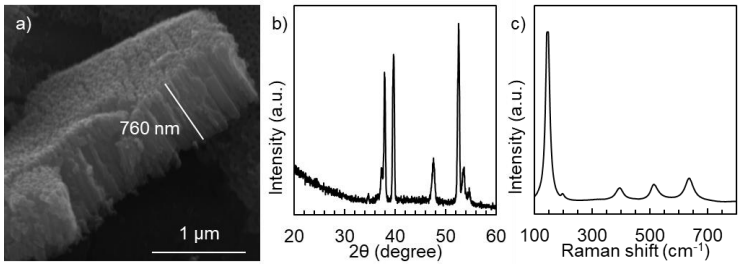

Figure 2: a) SEM picture, b) XRD pattern, and c) Raman spectra of TiO2 NTs

Photocurrent transients reported in Figure 3 show an anodic photocurrent, confirming the n-type semiconductor characteristics of the oxide. At approximately -0.5 V vs Ag/AgCl the photocurrent registered was close to zero, this value, as an estimate for the flat band potential, is in line with others documented in the literature (Pecoraro et al., 2024).

Figure 4 shows the EIS spectra obtained in a 0.5 M Na_2SO_4 solution at 0.5 V vs. Ag/AgCl. The setup involved employed TiO_2 NTs as the working electrode, Ni foam as the counter electrode and an Ag/AgCl reference electrode. The EIS spectra were carried out both in the absence and in the presence of 0.1 M glycerol, with and without UV irradiation. All the spectra were fitted by using the equivalent circuit in Figure 4. This circuit includes elements representing different parameters: R_s represents solution resistance, R_{CT} the charge transfer resistance, and $Q_{SC,el}$ the capacitance of TiO_2. The charge transfer resistance is related to the exchange current density that takes into account the kinetic constants (i.e., rate constants, k) of the oxidation reactions, in agreement with the specific reaction mechanism. The best fitting parameters are reported in Table 1.

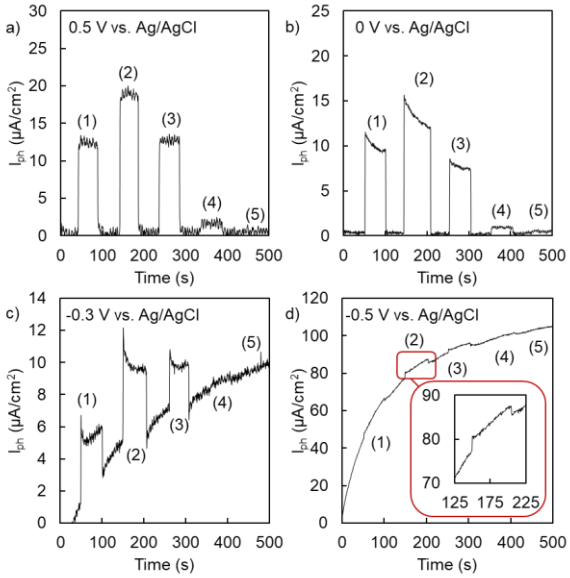

Figure 3: photocurrent transient executed at pH 7 and a) 0.5 V, b) 0 V, c) -0.3 V, and d) -0.5 V vs. Ag/AgCl using monochromatic light at various wavelength: (1) 300 nm, (2) 330 nm, (3) 350 nm, (4) 380 nm and (5) 400 nm.

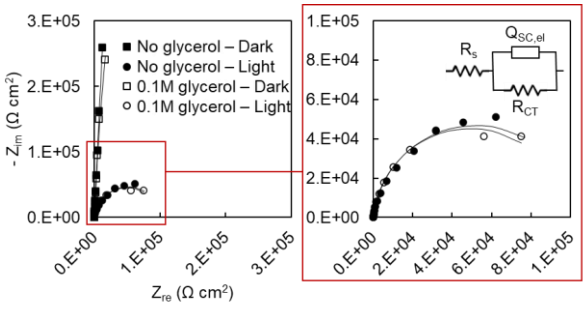

Figure 4: EIS spectra carried out at pH 7 and 0.5 V vs Ag/AgCl without and in the presence of glycerol and irradiation.

Table 1: Best fitting parameters of EIS spectra carried out at pH 7 and 0.5 V vs Ag/AgCl without and in the presence of glycerol and irradiation.

		No glycerol Dark	No glycerol Light	0.1 M Glycerol Dark	0.1 M Glycerol Light
R_s	(Ω cm^2)	96	86	73	73
R_{CT}	(Ω cm^2)	$4.4 \cdot 10^6$	$1.1 \cdot 10^5$	$4.0 \cdot 10^6$	$9.8 \cdot 10^4$
$Q_{sc,el}$	(S s^n cm^{-2})	$6.0 \cdot 10^{-6}$	$7.8 \cdot 10^{-6}$	$6.4 \cdot 10^{-6}$	$8.3 \cdot 10^{-6}$
n	(adm)	0.974	0.945	0.975	0.946

The influence of light irradiation on the electrode/electrolyte interface is notably evident except for R_s which shows a minor impact from both the irradiation and the presence of glycerol. Under dark conditions, the recorded R_{CT} is notably high. Additionally, the optimal fitting exponent 'n' for $Q_{sc,el}$ approximates 1, consistent with the

expected behavior of an almost perfect n-type semiconductor. During post-irradiation, a substantial reduction in R_{CT} occurs, closely linked to the amplified concentration of photocarriers and in agreement with the increased capacitance. However, during illumination, lower R_{CT} are recorded in a 0.1 M glycerol-containing solution compared to estimates in a glycerol-free solution. This confirms that, from a kinetic point of view, the overall reaction is less demanding under irradiation in the glycerol-containing solution.
Photoelectrocatalytic results are detailed in Table 2. Generally, under constant pH conditions, an increase in the applied bias results in an increase of the cell potential. Notably, at fixed applied bias, the cell potential increases as the pH increases. The same trends are observed for the photocurrent and thus for the reaction rates. This is consistent with the increased driving force, i.e., cell potential, caused by an increase of the applied bias, and a more favorable kinetic for OER at higher pH values.

Table 2: Photoelectrocatalytic results varying pH and applied bias.

pH	Applied bias (V vs. Ag/AgCl)	Cell potential (V)	Photocurrent (mA)	FE DHA (%)	FE GA (%)	FE CO_2 (%)	FE H_2 (%)
2	0.5	0.90	2.3	8.4	6.2	26	85
7	0.1	1.00	3.0	15.0	6.4	13	100
7	0.2	1.12	3.5	6.8	11.7	11	91
7	0.3	1.26	4.1	6.7	11.8	8	100
7	0.4	1.34	4.0	6.5	13.8	9	100
7	0.5	1.35	4.0	7.4	16.9	12	84
7	1.0	1.85	5.4	9.5	15.2	6	85
14	0.1	1.20	4.7	1.1	0	0	96
14	0.3	1.39	4.8	1.7	0	0	51
14	0.5	1.57	5.0	3.8	0	0	41

The partial oxidation products, specifically DHA and GA, show different FEs depending on the pH of the reaction mixture. Significantly, the highest FE for DHA and GA was obtained at pH 7 with an applied bias of 0.1 V and 0.5 V vs Ag/AgCl respectively. Moreover, at higher pH, the DHA production is reduced, and it drops to 0 for GA. This may be due to the increased OER at higher pH values, thanks to its favorable kinetic, which in turn hinders the production of HVA products derived by glycerol photooxidation.
CO_2 production, indicative of glycerol mineralization, is strongly affected by the pH of the reaction mixture rather than the cell potential. Notably, FE towards CO_2 stands at 26 % at pH 2, approximately 10 % at pH 7, and drops to 0 at pH 14. This trend aligns with the hypothesis that the applied bias mainly serves to minimize recombination between photoinduced holes and electrons, rather than affecting their potential. Conversely, the pH influences the redox potential of species within the reaction mixture as well as the kinetic toward the OER, affecting the glycerol mineralization to CO_2 and H_2.
The FE towards H_2 diminishes as both the pH and the applied bias increase. This observation aligns with findings in the literature and is likely linked to higher O_2 production, which interacts with the generated H_2, thereby reducing its FE (Hunsom et al., 2013; Karimi Estahbanati et al., 2019). A higher bias as well as a higher pH favours the kinetic of oxygen evolution. Indeed, this reaction is kinetically sluggish and thus more sensitive to the electric field at across the space charge region of the semiconductor (namely TiO_2). The electric field in turn raises by raising the potential with respect to the flat band potential. Since O_2 can diffuse to the cathode its reduction becomes competitive with respect to H_2 evolution thus explain the experimental findings.

4. Conclusions

This study investigates the influence of pH and applied bias for H_2 production and HVA products from glycerol photooxidation in a photoelectrochemical cell. TiO_2 NTs measuring 760 nm length over 24 cm^2 as the surface area were used as the photoanode and PGM-free Ni foam of 6 cm^2 as the cathode.
Photoelectrocatalytic tests were carried out across acidic, neutral, and basic pH, employing applied bias ranging from 0.1 and 1 V vs Ag/AgCl. The results show the highest FE towards HVA products, i.e., DHA and GA at pH 7 and applied bias of 0.5 V and 0.1 V vs. Ag/AgCl respectively, remaining stable at higher applied bias. The highest glycerol photoreforming level was obtained at lower pH. Conversely, at higher pH, both the glycerol photooxidation and photoreforming, i.e., FE towards DHA, GA, and CO_2, decreased, and I_{ph} increased. This suggest that water splitting is more pronounced at higher pH, resulting in a lower FE towards H_2 because of the subsequent reaction with the O_2 in the gas phase.
As final remark, it is important to stress that these results are encouraging considering the high chemical and physical stability of the employed PGM free electrodes, offering interesting perspectives for future developments

in targeted applications (i.e., H_2 production and/or HVA products) and opens up new routes for sustainable technologies.

Nomenclature

EIS – Electrochemical Impedance Spectroscopy
FE – faradaic efficiency
HVA – High Value Added
NTs – Nanotubes
OER – Oxygen Evolution Reaction
PGM – Platinum metal group

Acknowledgments

C.M.P. acknowledges support from the University of Palermo.

References

Albu, S. P., Tsuchiya, H., Fujimoto, S., & Schmuki, P. (2010). TiO_2 Nanotubes – Annealing Effects on Detailed Morphology and Structure. European Journal of Inorganic Chemistry, 2010(27), 4351–4356. https://doi.org/10.1002/ejic.201000608

Balachandran, U., & Eror, N. G. (1982). Raman spectra of titanium dioxide. Journal of Solid State Chemistry, 42(3), 276–282. https://doi.org/10.1016/0022-4596(82)90006-8

Dey, A., Houle, F. A., Lubner, C. E., Sevilla, M., & Shaw, W. J. (2021). Introduction to (photo)electrocatalysis for renewable energy. Chemical Communications, 57(13), 1540–1542. https://doi.org/10.1039/D0CC90530E

Hunsom, M., & Saila, P. (2013). Product Distribution of Electrochemical Conversion of Glycerol via Pt Electrode: Effect of Initial pH. Int. J. Electrochem. Sci, 8, 11288–11300. www.electrochemsci.org

Karimi Estahbanati, M. R., Mahinpey, N., Feilizadeh, M., Attar, F., & Iliuta, M. C. (2019). Kinetic study of the effects of pH on the photocatalytic hydrogen production from alcohols. International Journal of Hydrogen Energy, 44(60), 32030–32041. https://doi.org/10.1016/J.IJHYDENE.2019.10.114

Kong, P. S., Aroua, M. K., & Daud, W. M. A. W. (2016). Conversion of crude and pure glycerol into derivatives: A feasibility evaluation. Renewable and Sustainable Energy Reviews, 63, 533–555. https://doi.org/10.1016/j.rser.2016.05.054

Luo, L., Chen, W., Xu, S.-M., Yang, J., Li, M., Zhou, H., Xu, M., Shao, M., Kong, X., Li, Z., & Duan, H. (2022). Selective Photoelectrocatalytic Glycerol Oxidation to Dihydroxyacetone via Enhanced Middle Hydroxyl Adsorption over a Bi_2O_3 -Incorporated Catalyst. Journal of the American Chemical Society, 144(17), 7720–7730. https://doi.org/10.1021/jacs.2c00465

Pecoraro, C. M., Bellardita, M., Loddo, V., Di Franco, F., Palmisano, L., & Santamaria, M. (2023). A facile way to synthesize noble metal free TiO_2 based catalysts for glycerol photoreforming. Journal of Industrial and Engineering Chemistry, 118, 247–258. https://doi.org/10.1016/j.jiec.2022.11.010

Pecoraro, C. M., Bellardita, M., Loddo, V., Virtù, D., Di Franco, F., & Santamaria, M. (2023). Photocatalytic and photoelectrocatalytic H_2 evolution combined with valuable furfural production. Applied Catalysis A: General, 650, 118987. https://doi.org/10.1016/j.apcata.2022.118987

Pecoraro, C. M., Di Franco, F., Bellardita, M., Loddo, V., & Santamaria, M. (2024). Enhancing H_2 production rate in PGM-free photoelectrochemical cells by glycerol photo-oxidation. International Journal of Hydrogen Energy, 49, 322–336. https://doi.org/10.1016/j.ijhydene.2023.08.011

Pitchaimuthu, S., Sridharan, K., Nagarajan, S., Ananthraj, S., Robertson, P., Kuehnel, M. F., Irabien, Á., & Maroto-Valer, M. (2022). Solar Hydrogen Fuel Generation from Wastewater—Beyond Photoelectrochemical Water Splitting: A Perspective. Energies, 15(19). https://doi.org/10.3390/EN15197399

Reyes-Coronado, D., Rodríguez-Gattorno, G., Espinosa-Pesqueira, M. E., Cab, C., de Coss, R., & Oskam, G. (2008). Phase-pure TiO_2 nanoparticles: anatase, brookite and rutile. Nanotechnology, 19(14), 145605. https://doi.org/10.1088/0957-4484/19/14/145605

Santamaria, M., Conigliaro, G., Franco, F. Di, Megna, B., & Quarto, F. Di. (2017). Electronic Properties of Thermal Oxides on Ti and Their Influence on Impedance and Photoelectrochemical Behavior of TiO_2 Nanotubes. Journal of The Electrochemical Society, 164(4), C113–C120. https://doi.org/10.1149/2.0601704jes

Verma, A. M., Laverdure, L., Melander, M. M., & Honkala, K. (2022). Mechanistic Origins of the pH Dependency in Au-Catalyzed Glycerol Electro-oxidation: Insight from First-Principles Calculations. ACS Catalysis, 12(1), 662–675. https://doi.org/10.1021/ACSCATAL.1C03788/ASSET/IMAGES/LARGE/CS1C03788_0006.JPEG

Yao, T., An, X., Han, H., Chen, J. Q., & Li, C. (2018). Photoelectrocatalytic Materials for Solar Water Splitting. Advanced Energy Materials, 8(21), 1800210. https://doi.org/10.1002/AENM.201800210